

# Synthesis of Clean Hydrogen Gas from Waste Plastic at Zero Net Cost

Kevin M. Wyss, Karla J. Silva, Ksenia V. Bets, Wala A. Algozeeb, Carter Kittrell, Carolyn H. Teng, Chi Hun Choi, Weiyin Chen, Jacob L. Beckham, Boris I. Yakobson,\* and James M. Tour\*

Hydrogen gas (H<sub>2</sub>) is the primary storable fuel for pollution-free energy production, with over 90 million tonnes used globally per year. More than 95% of H<sub>2</sub> is synthesized through metal-catalyzed steam methane reforming that produces 11 tonnes of carbon dioxide (CO<sub>2</sub>) per tonne H<sub>2</sub>. “Green H<sub>2</sub>” from water electrolysis using renewable energy evolves no CO<sub>2</sub>, but costs 2–3× more, making it presently economically unviable. Here catalyst-free conversion of waste plastic into clean H<sub>2</sub> along with high purity graphene is reported. The scalable procedure evolves no CO<sub>2</sub> when deconstructing polyolefins and produces H<sub>2</sub> in purities up to 94% at high mass yields. The sale of graphene byproduct at just 5% of its current value yields H<sub>2</sub> production at a negative cost. Life-cycle assessment demonstrates a 39–84% reduction in emissions compared to other H<sub>2</sub> production methods, suggesting the flash H<sub>2</sub> process to be an economically viable, clean H<sub>2</sub> production route.

of CO<sub>2</sub> production annually, equal to the annual CO<sub>2</sub> emissions of the United Kingdom.<sup>[1]</sup> H<sub>2</sub> demand is projected to grow rapidly throughout the next three decades (Figure 1a), so alternative production methods are needed to mitigate further CO<sub>2</sub> emissions.<sup>[2]</sup> Electrolysis of water to produce H<sub>2</sub> (“green hydrogen”) and oxygen (O<sub>2</sub>) presents one such pathway, affording little greenhouse gases when powered by renewable energy.<sup>[3]</sup> Disappointingly, despite current emissions consciousness, electrolysis affords <5% of global H<sub>2</sub> production because of its high cost (Figure 1b)<sup>[4]</sup>; expensive metal catalysts, such as Pt, Ir, or Ru, are often required.<sup>[5]</sup> For every 1 tonne of H<sub>2</sub> produced, 9 tonnes of fresh water are consumed, limiting the implementation of electrolysis in some locales.<sup>[6]</sup>

## 1. Introduction

Hydrogen gas (H<sub>2</sub>) constitutes an attractive energy technology due to its high efficiency in fuel cells and greenhouse gas-free combustion. Ironically, however, 95% of global H<sub>2</sub> is produced by steam methane reforming (called “grey hydrogen”) which evolves 11 tonnes of carbon dioxide (CO<sub>2</sub>) per 1 tonne of H<sub>2</sub>. That singular process is responsible for 800 million tonnes (MT)

High-temperature methane pyrolysis to form H<sub>2</sub> plus solid carbon (“turquoise hydrogen”), and steam methane reforming with associated CO<sub>2</sub> capture (“blue hydrogen”), do not result in the release of stoichiometric greenhouse gases but they still require fossil-fuel feedstocks and not yet economically competitive with traditional grey hydrogen.<sup>[7,8]</sup>

Ideally, low-cost H<sub>2</sub> production methods are needed that evolve little CO<sub>2</sub>, require no costly catalysts, and use abundant feedstocks.<sup>[9]</sup> In 2021, the US Department of Energy targeted the production of 1 kg of H<sub>2</sub> for \$1 in 1 decade, the so-called “1:1:1” goal.<sup>[10]</sup> The co-production of H<sub>2</sub> with high-value materials could afford an economic basis to achieve this goal, and thereby displace steam methane reforming (Figure 1c). Concurrently, waste plastics are up to 14 wt.% atomic H and are widely available since 380 MT are produced annually, plus there are enormous backlogs of accumulated waste plastics.<sup>[11]</sup> Consequently, several technologies have viewed waste plastic as a source of H<sub>2</sub>. Typically, plastic pyrolysis converts waste plastics into small hydrocarbons, which are then steam-reformed to yield H<sub>2</sub>, carbon monoxide (CO), and CO<sub>2</sub>.<sup>[12,13]</sup> These reactions further require complex catalysts. Recent research has demonstrated the use of FeAlO<sub>x</sub> with microwaves to degrade polyolefins into H<sub>2</sub>, light olefins, and impure carbon nanotubes due to rapid heating rates, but the iron aluminum oxide (FeAlO<sub>x</sub>) is required in equal weight to waste plastic feedstock and the microwave energy input is large.<sup>[14]</sup>

In this work, we show that rapid flash Joule heating (FJH) of waste plastic can be performed with no added catalyst to

K. M. Wyss, K. J. Silva, W. A. Algozeeb, C. Kittrell, C. H. Teng, C. H. Choi, W. Chen, J. L. Beckham, J. M. Tour  
Department of Chemistry  
Rice University  
6100 Main Street, Houston, TX 77005, USA  
E-mail: tour@rice.edu

K. V. Bets, B. I. Yakobson, J. M. Tour  
Department of Materials Science and NanoEngineering  
Rice University  
6100 Main Street, Houston, TX 77005, USA  
E-mail: bij@rice.edu

B. I. Yakobson, J. M. Tour  
Smalley-Curl Institute  
NanoCarbon Center and the Rice Advanced Materials Institute  
Rice University  
6100 Main Street, Houston, TX 77005, USA

The ORCID identification number(s) for the author(s) of this article can be found under <https://doi.org/10.1002/adma.202306763>

DOI: 10.1002/adma.202306763

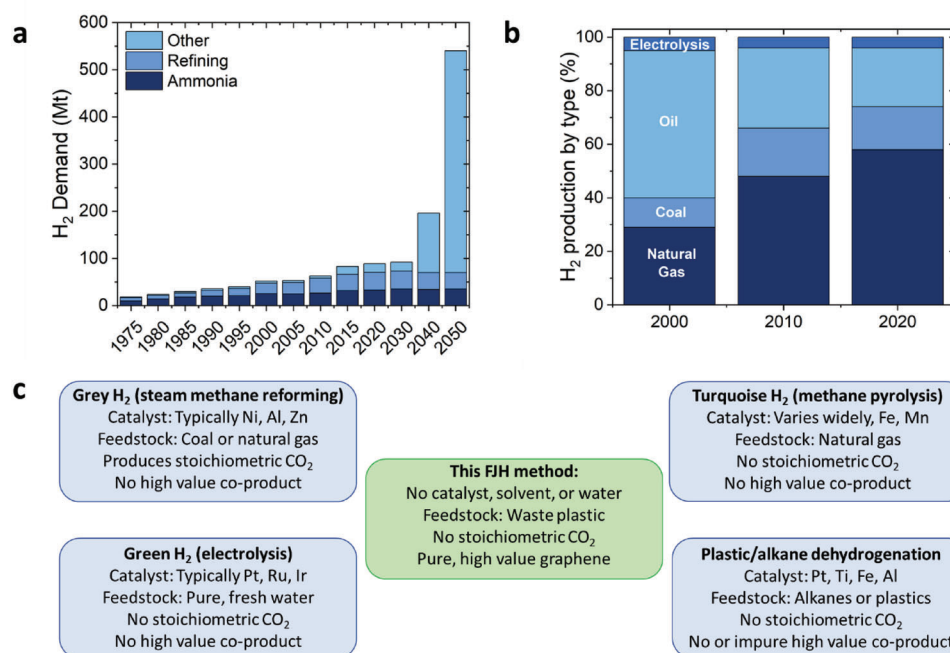


**Figure 1.** The current state of H<sub>2</sub> production and projected demand. a) Historic and projected demand for H<sub>2</sub>, separated by use. b) The source of hydrogen historically produced, separated by feedstock. c) A scheme comparing the other H<sub>2</sub> production methods with the flash H<sub>2</sub> process presented here.

deconstruct polyolefins, polyesters, and mixed waste plastics, affording high yields of H<sub>2</sub> (that we refer to as “flash H<sub>2</sub>”) along with high purity graphene as a value-added byproduct. Based on the sale of the graphene byproduct of this FJH H<sub>2</sub>-production process, the H<sub>2</sub> produced by this process has negative production cost, even if the graphene is sold at <5% (US\$3000 per tonne) of its current market cost of US\$60 000–US\$100 000 per tonne. Moreover, a life-cycle assessment shows that the FJH of polyolefins produces “clean H<sub>2</sub>” as defined by the US Department of Energy by generating <4 kg CO<sub>2</sub> per 1 kg H<sub>2</sub>. Flash H<sub>2</sub> uses less energy than green or turquoise H<sub>2</sub> while producing less greenhouse gas emissions than grey, blue, and turquoise H<sub>2</sub>. Therefore, this catalyst-free flash H<sub>2</sub> route removes mixed waste plastic streams, upcycling them into graphene, while generating up to 47 mol of H<sub>2</sub> per kg of input plastic, all at an overall negative cost for this clean H<sub>2</sub> fuel source.

## 2. Results and Discussion

### 2.1. Optimization of Catalyst-Free Polyethylene Deconstruction

FJH leverages rapid current discharge through a resistive feedstock to achieve heating within the resistor, removing slow heat transfer steps, allowing for heating rates up to 10<sup>5</sup> K s<sup>-1</sup> and achieving peak temperatures of ≈3100 K.<sup>[15,16]</sup> A general scheme of the methods used here is presented in Figure 2a and Figures S1, S2 (Supporting Information). The resistance of the sample limits the magnitude of current by Ohm’s law, controlling the amount of heat generated. Here, capacitors supply the current, but alternating current (AC) voltage sources can also be used.<sup>[17–19]</sup> Plastics are electrically insulating thus requiring conductive additives to be mixed in, thereby forming a conductive

path between the polymer grains.<sup>[20]</sup> Low (3–5 wt.%) amounts of conductive additives, such as carbon black, result in higher resistances, limiting the amount of current discharge and therefore heat generated, while 16 wt.% additive results in lower feedstock resistances, higher reaction temperatures, and faster current discharge (Figure 2b).

Iterative current discharges are used to heat the plastic waste sample. The current discharged through the sample can be measured by a Hall effect sensor. Through iterative discharges, the resistance of the sample decreases as the plastic is carbonized, resulting in higher currents and faster discharge. A jagged, interrupted current is observed in the first three discharges due to the outgassing of volatiles momentarily pushing the spring-loaded electrodes apart, intermittently opening the circuit. A smooth fourth current discharge demonstrates no more outgassing (Figure 2a). These volatiles are trapped, and then studied by gas chromatography with thermal conductivity and mass spectrometer detectors. The volatiles are collected over all four current discharges and analyzed in entirety as the mixture. In a typical experiment converting polyethylene/conductive additive mixture at 6 Ohm initial resistance into graphene and volatiles, the volatile trap is purged with Ar gas, and then evacuated to –75 kPa. Then, over the course of the FJH discharge, the volatile gas trap with a total volume of 100 mL achieves a pressure of +250 kPa for a typical total pressure change of +325 kPa. This pressure change would depend on the size of the volatile gas trap. Collection of the gas at ambient conditions was not conducted so that the volatiles could be studied without air contamination.

The produced volatile streams contain large amounts of H<sub>2</sub>, along with other hydrocarbons. Post-consumer waste high-density polyethylene (HDPE) was used to optimize the process. Production of H<sub>2</sub> was found to correlate with the initial

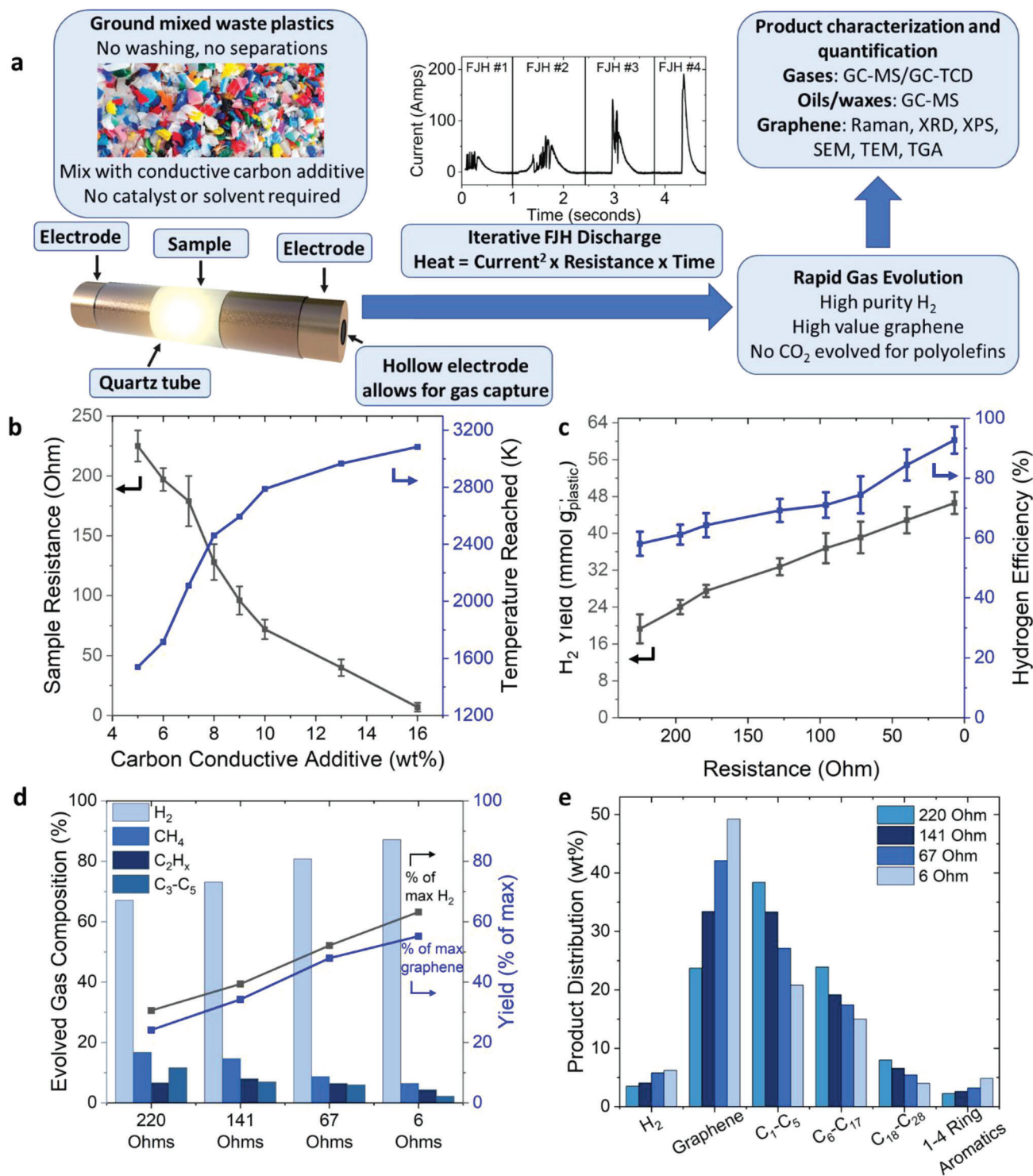


**Figure 2.** Catalyst-free deconstruction of polyethylene to yield flash H<sub>2</sub> and graphene. a) A schematic showing the typical flash Joule heating process used to convert waste plastic into flash H<sub>2</sub>, with the inset graph showing the current discharge as a function of time over four iterative FJH treatments at 6 Ohm initial resistance samples to deconstruct the waste plastic. b) The resistance of the plastic sample before treatment (black trace) and peak temperature reached during FJH treatment (red trace) as a function of conductive carbon black mixed with waste polyethylene. Error bars represent the standard deviation,  $N = 3$ . c) The relationship between initial sample resistance, H<sub>2</sub> yield (black trace), and hydrogen efficiency (red trace) in the FJH deconstruction of polyethylene. Hydrogen efficiency is the total mass of atomic hydrogen contained in all gas phase products, as compared to the atomic hydrogen content of the starting polymer. Error bars represent the standard deviation,  $N = 3$ . d) The relationship between initial sample resistance and the gaseous products and yield of H<sub>2</sub> and graphene resulting from polyethylene deconstruction, where the bar graph corresponds to the partial pressure of the gas, while the line graph corresponds to the yield of H<sub>2</sub> (black trace) or graphene (blue trace) compared to the amount of atomic H and C present in the starting mixture. e) Mass balance of polyethylene deconstruction as resistance varies.

sample resistance; lower resistances resulting in higher H<sub>2</sub> production, indicating that higher peak temperature, faster heating rates, and shorter discharge durations increase H<sub>2</sub> yield. Hydrogen efficiency has previously been defined as the total mass of atomic hydrogen contained in all gas phase products, as compared to the atomic hydrogen content of the starting polymer.<sup>[14]</sup> Hotter, faster heating rates result in more H<sub>2</sub> recovered and more atomic hydrogen liberated from solid polymer (Figure 2c), and up to 46.6 mmol H<sub>2</sub> per g of HDPE, 92.7% efficiency, and 87% gas purity are obtained when the initial resistance is 6 Ohm. Other gases are produced, predominantly consisting of methane and short alkenes. As higher temperatures and faster heating rates are reached, the purity of the flash H<sub>2</sub> increases (Figure 2d, bar graph). In an ideal reaction, all carbon atoms in the polyethylene would convert to graphene, while all hydrogen atoms would be released as H<sub>2</sub>. The percentage yield versus this ideal maximum is also plotted in Figure 2d (line graph).

A complete mass balance is required to understand what other products result from the deconstruction. Figure 2e shows the mass yield of flash H<sub>2</sub>, graphene, hydrocarbon gases, oils, waxes, and aromatic residues produced by the FJH deconstruction. Again, hotter and faster reactions favor more complete polymer deconstruction, resulting in lower hydrocarbon gas, oil, and wax production, with higher graphene and H<sub>2</sub> yields at lower sample resistances.

## 2.2. Characterization of Upcycled Graphene Byproduct

The carbon atoms left behind by the evolution of H<sub>2</sub> from waste plastic are rearranged into the 2D nanomaterial graphene. Graphene, with its high strength and conductivity, has been studied extensively since its isolation.<sup>[21,22]</sup> A multitude of demonstrated graphene applications exist, including composites with concrete, asphalt, and plastics, as well as gas and water filtration, energy storage devices, and flexible electronics, with industrial-scale implementation being realized in 2018 by Ford Motor Company. Graphene is in all Ford automobiles since February 2020, predominantly in the foam cushion seats and under-hood insulation.<sup>[23–25]</sup> Single- or few-layered graphene sheets have high value due to current worldwide production limitations of only 15 tons per day.<sup>[26]</sup> As the price declines, extensive use is projected in many large-scale construction materials markets.

Low defect content, few-layer composition, and high carbon content are favorable properties for graphene applications.<sup>[27]</sup> Raman spectroscopy is the most common method to characterize graphene since it can inform the quality, layering, and orientation based on major peaks including the D peak at  $\approx 1350\text{ cm}^{-1}$  indicating lattice defect content, G peak at  $\approx 1600\text{ cm}^{-1}$  indicating sp<sup>2</sup>-hybridized character, and 2D peak at  $\approx 2690\text{ cm}^{-1}$  indicating graphene sheet layering.<sup>[28]</sup> Since large amounts of graphene nanocrystals are produced with each reaction, large-area Raman spectral analysis allows for the analysis of 100 different spectra to provide a representative single spectrum with standard deviation and graphene purity determination (Figure 3a,b). Lower feedstock resistances result in better graphene quality, determined by defect content (D peak intensity) and graphene lattice quality (2D peak intensity, shape, position, and width), as well as higher product purity of 97–99% graphene. Since lower resistances re-

sult in higher reaction temperatures, more annealed graphene sheets, and less amorphous carbon result.

Deconstruction of waste polyethylene can be followed by powder X-ray diffraction (XRD), showing near-complete conversion to graphene over the optimized FJH process (Figure 3c). The powder XRD also shows a broadening of the graphene (002) peak consistent with few-layer graphene, and little detectable residual crystalline impurities.<sup>[29]</sup> Since no catalyst is used and only small amounts of carbon additive are required, the graphene product has high carbon purity and sp<sup>2</sup>-hybridization, as probed by X-ray photoelectron spectroscopy, unlike similar plastic deconstruction processes, suggesting that no further purification or processing is required prior to graphene use (Figure 3d). The thermogravimetric analysis also indicates high-purity graphene formation; a single and complete degradation is observed at 680 °C under air atmosphere, showing no residual inorganic or polymer content (Figure S3, Supporting Information). Large, highly crystalline, sheet-like morphologies of waste plastic-derived graphene are observed by scanning electron microscopy imaging (Figure 3e). Transmission electron microscopy demonstrates few-layer thickness and turbostratic stacking (Figure S4, Supporting Information).

Exfoliation of graphene and its dispersion are essential considerations in composite, anode, or device fabrication. Turbostratic, or rotationally disordered, layering of graphene sheets disrupts the interlayer  $\pi$ - $\pi$  interactions providing unique electronic and magnetic properties, significantly lowering the barrier for graphene sheet exfoliation.<sup>[30,31]</sup> Rapid heating and cooling rates kinetically trap the graphene byproduct as turbostratic graphene, apparent through high-resolution Raman spectroscopic analysis. The appearance of TS<sub>1</sub> and TS<sub>2</sub> peaks and the missing M peak signify turbostratic graphene, resulting in superior dispersibility when compared to commercial graphene made by graphite exfoliation, which displays ordered AB-stacking and the expected M peak by Raman analysis (Figure 3f; Figure S5, Supporting Information).<sup>[32]</sup>

Graphene formed by the FJH method has been leveraged in many demonstrated applications, including composites, energy storage in Li batteries, and electrocatalysis.<sup>[19,29,33]</sup> In  $\approx 3$  years, FJH production of graphene has increased from 1 g per hour to >1 kg per hour rates at the laboratory scale, while the industry has achieved pilot plant tonne-per-day rates.<sup>[34]</sup> Feedstocks besides waste plastics should also be considered, ideally high in atomic H content and low in atomic O content to minimize CO<sub>2</sub> evolution. Asphalt, bitumen, and asphaltenes contain >11% H and <1% O, and they present large-scale, low-cost materials that can supplement plastic deconstruction for H<sub>2</sub> production if necessary.<sup>[35]</sup> Asphaltenes are demonstrated here to also produce high-purity H<sub>2</sub> and graphene byproducts (Figure S6, Supporting Information).

## 2.3. Process Generality for Catalyst-Free Deconstruction of Mixed Polymers

Although polymer recycling methods have existed for decades, 95% of produced plastic is never recycled due to the high cost of manually separating the diverse plastic types, large amounts of water and detergent required for washing prior to re-melting,

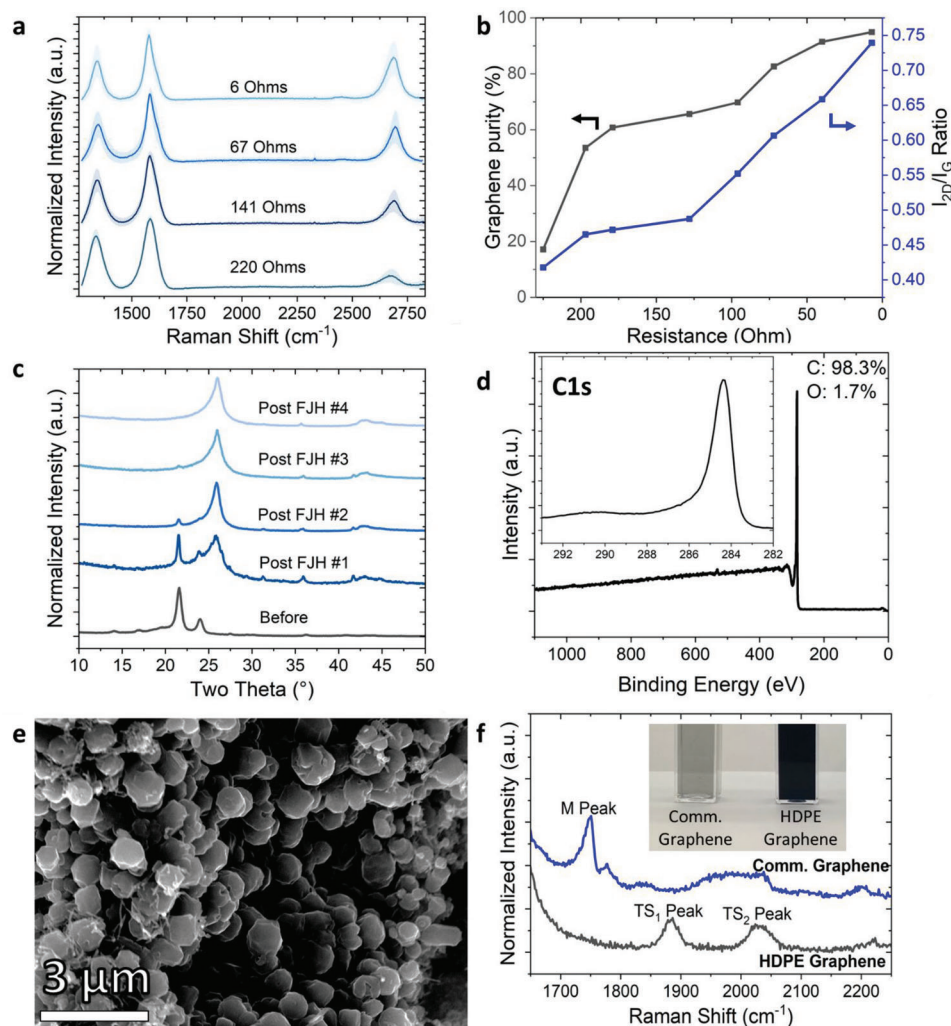


**Figure 3.** Characterization of polyethylene-derived graphene. a) The average Raman spectra (100 unique spectra, over a 1 mm<sup>2</sup> area) of graphene produced as initial polyethylene sample resistance is varied. The standard deviation is represented by the shaded area. b) Raman spectroscopy determined graphene purity and  $I_{2D}/I_G$  ratio as a function of sample resistance, showing the average of 100 unique spectra per sample. c) Bulk powder X-ray diffraction analysis of solid produced from a 6 Ohm sample of polyethylene over iterative FJH treatment, as compared to the initial feedstock mixture, showing bulk conversion of polyethylene into pure graphene. d) X-ray photoelectron spectroscopy analysis of a 6 Ohm sample produced graphene, with inset high-resolution analysis of the C1s transition. e) Scanning electron micrograph of crystalline graphene produced from a 6 Ohm sample of polyethylene. f) High-resolution Raman spectra demonstrating the presence of the TS<sub>1</sub> and TS<sub>2</sub> peaks in FJH graphene samples indicating turbostratic stacking, while the presence of the M peak in commercial graphene samples indicates AB stacking. An inset photograph shows polyethylene-derived graphene and commercial graphene dispersed in water-Pluronic (F-127) solution (1 wt.%) by sonication and centrifuged, showing turbostratic stacking significantly improves graphene dispersibility.

and an inferior recycled polymer product when compared to virgin plastics. Since the FJH process needs no catalyst, we hypothesized that it would proceed similarly with any feedstock. **Figure 4a** shows that hydrogen efficiency is not substantially impacted by the polymer identity. Since other polymers screened contain less atomic hydrogen than HDPE, it is expected that less H<sub>2</sub> per gram of polymer is recovered. The purity of H<sub>2</sub> resulting from all polyolefins is >84%. Some CO and CO<sub>2</sub> are produced when polyesters are deconstructed, resulting from oxygen present in the ester linkages. Similarly, some N<sub>2</sub> is produced when N-containing polymers such as acrylonitrile-butadiene-styrene (ABS) are deconstructed (**Figure 4b**).

Mixed waste plastic can be readily deconstructed without any separation or washing. The FJH process achieves 52–68% yields for H<sub>2</sub>, and 46–63% yields for graphene for all polymers and mixes studied, outperforming other catalyst-free deconstruction methods by 5–10×. Polystyrene produces the highest purity H<sub>2</sub> stream since the aromatic stability of the styrene minimizes the formation of gaseous hydrocarbons.

Instead of carbon black, low-value conductive additives were studied to decrease costs upon process scale-up. Waste ash resulting from the pyrolysis of plastics, charcoal, and metallurgical coke (metcoke) were used, and **Figure 4c,d** shows that the identity of the conductive additive does not affect flash H<sub>2</sub>

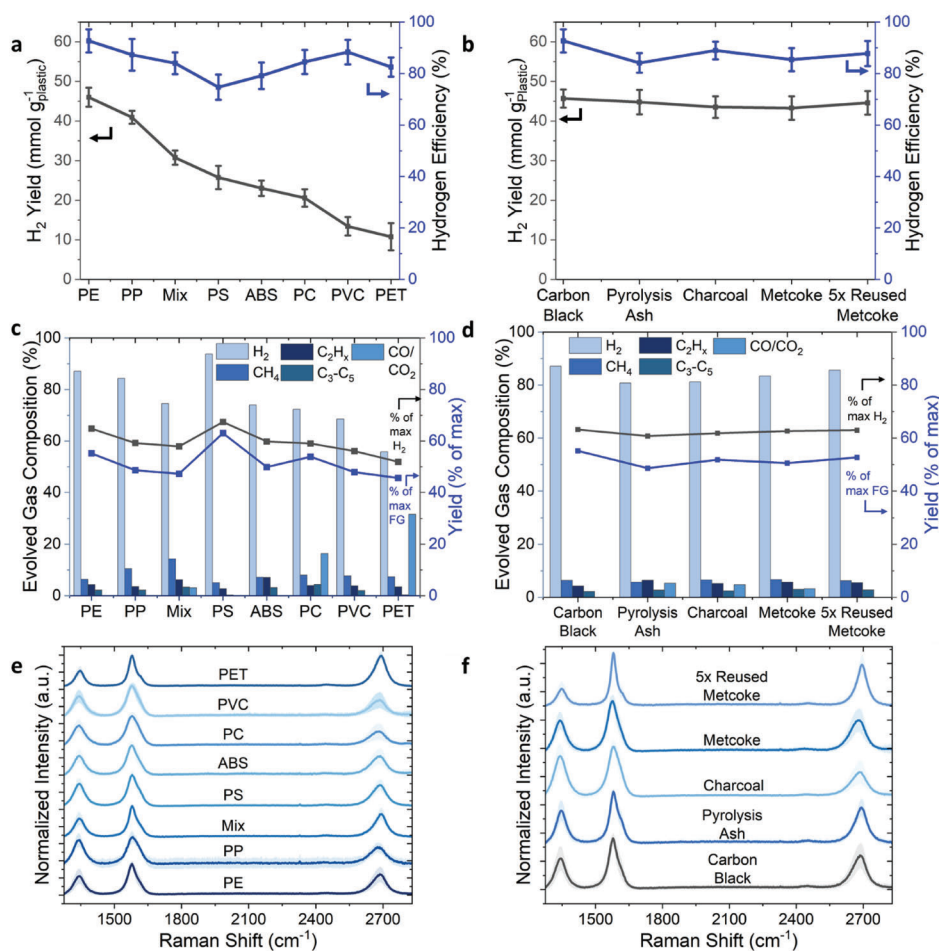


**Figure 4.** Process generality for other waste polymers, mixtures, and low-cost conductive additives. a) Flash H<sub>2</sub> yield (black) and efficiency (blue) as waste plastic type varies. Error bars represent the standard deviation,  $N = 3$ . b) Flash H<sub>2</sub> yield (black) and efficiency (blue) as conductive additive varies. Error bars represent the standard deviation,  $N = 3$ . c, d) Gaseous products evolved, with flash H<sub>2</sub> and graphene yields calculated, as c) waste plastic type or d) conductive additives are varied. The bar graph corresponds to the partial pressure of gas, while the line graph corresponds to the yield of flash H<sub>2</sub> (black) or graphene (blue) compared to the amount of atomic H and C present in the starting mixture. e, f) Average Raman spectra (100 unique spectra, over a 1 mm<sup>2</sup> area) as e) waste plastic type or f) conductive additive varies. The shaded area represents the standard deviation in spectra. The “Mix” contains 20% low-density polyethylene (LDPE), 20% high-density polyethylene (HDPE), 15% polystyrene (PS), 10% polyvinylchloride (PVC), and 15% polyethylene terephthalate (PET). Other polymers tested include ABS and polycarbonate (PC).

efficiency or yields. Small amounts of CO and CO<sub>2</sub> are produced when the conductive additive has atomic O content. Metcoke can be repeatedly used as a conductive additive through simple sieve separation, further lowering costs associated with the conductive additive, with 92% of the metcoke recovered after 5 use cycles. The metcoke is converted to graphene after the first cycle but remains in large particles thus facilitating separation. Further, after the first cycle, no CO or CO<sub>2</sub> is produced since the O content has been removed (Figure 4d). Graphene quality is largely unaffected by both polymer and conductive additive types (Figure 4e,f).

Upon hypothetical scale-up of this H<sub>2</sub> production method, and the batch size during FJH is increased, the risk of combustion or ignition of the produced volatiles will also increase. At the lab scale, this is avoided by using an evacuated ballast, in the form of a Schlenk flask evacuated to  $-75$  kPa which removes any O<sub>2</sub> required for combustion or ignition, as well as rapidly removing the volatiles from the high-temperature reaction area. Suitable

engineering controls for gas capture and partition away from the reaction space, followed by purification will be required upon further scaleup.

#### 2.4. Computational and Experimental Mechanistic Study of FJH Process

Since no catalyst is present during the rapid FJH, the generation of flash H<sub>2</sub> likely proceeds through C–H bond homolysis which deconstructs the polymer chains into the observed volatiles (Figure S7, Supporting Information). The ultrafast heating rates and high temperatures (Figure 2b) allow for more complete deconstruction into the most thermodynamically favored products (Figure S8, Supporting Information). The reaction mechanism for the FJH or laser vaporization-assisted transformation of amorphous or olefinic carbon into graphene

has been previously attributed to mobile carbon nucleating the sheets through a seed-growth mechanism, which can achieve diffusion-controlled reaction kinetics at sufficiently high energy density.<sup>[29,36–38]</sup>

The growth of semicrystalline turbostratically stacked sheet-like graphene domains from small, wrinkled, and defective regions can be observed morphologically by SEM imaging as the sample resistance decreases (Figure 5a). Large areas of sheet-like morphologies are not observed until reaching temperatures >2300 K, corresponding to an atomic C vapor pressure of  $\approx 10^{-4}$  Pa. This low vapor pressure, maintained for only milliseconds, is unlikely to allow for micron-scale crystal growth, indicating another intermediate is required for the mobile carbon hypothesis.<sup>[39]</sup> The FJH process forms 1,3-butadiene, ethylene, and benzene as detected by GC-mass spectrometry (GC-MS), which can combine through aromatic polymerization, forming graphitic domains (Figure S9, Supporting Information). Aromatic products are detected, with the overall amount and size of aromatics increasing as resistance is lowered and higher temperatures are achieved (Figure 5b). Polymerization of polyaromatic hydrocarbons has been previously demonstrated under high energy density conditions, such as in stars or under laser irradiation.<sup>[40,41]</sup> The detected polyaromatic hydrocarbons formed during FJH can be considered the seeds of eventual turbostratic graphene sheets, which grow through the aromatic coupling of other mobile carbon species.

These findings are also studied computationally through molecular dynamics (MD) simulations with AIREBO interatomic potentials.<sup>[42,43]</sup> Following the structural characteristics of the HDPE, the system of long, highly intertwined PE strands was constructed.<sup>[44]</sup> Due to the high flexibility of the polymer chains at temperatures observed during FJH, smaller structures or those containing shorter chains displayed rapid unraveling mandating the use of chains with at least 150 carbon atoms.<sup>[45]</sup> The HDPE structure was generated through the iterative addition of carbon strands composed of a series of randomly oriented straight and curved segments, ensuring a significantly interwoven configuration (Figure 5c,d). Following experimental results, we compared the system behavior at 1500 and 3000 K, representing samples with high (225 Ohm) and lower (30 Ohm) resistance, respectively. In both cases, the evolution of H<sub>2</sub> and the synthesis of short-chain hydrocarbons was observed throughout the simulation, with H<sub>2</sub> production significantly increased at higher temperatures (Figure 5e). The dehydrogenated and partially dehydrogenated carbon chains formed bonds producing interconnected carbon networks and aromatic segments (Figure 5f), further proceeding to the formation of graphitic domains.

### 2.5. Life-Cycle Assessment and Techno-economic Analysis of Upcycling Process

Life-cycle assessment (LCA) is a technique used to analyze the holistic environmental impacts and resource demands associated with production methods, allowing for direct comparisons.<sup>[46,47]</sup> The LCA conducted here compares the cradle-to-gate inputs, outputs, and demands associated with producing a functional unit of 1 kg of purified H<sub>2</sub> by various methods. LCA for the conversion of polyethylene into flash H<sub>2</sub> by the FJH process and a recently

reported catalytic microwave-irradiation polymer deconstruction process are compared to the LCAs of other common H<sub>2</sub> production methods. Techno-economic analysis (TEA) similarly considers the associated costs and thus estimates and compares the economic feasibility of processes. Further details regarding the FJH and microwave deconstruction LCAs and TEAs can be found in the Experimental Section (Supporting Information), Figures S10, S11 and Tables S1–S3 (Supporting Information). The costs and burdens associated with the purification of the mixed volatile gas stream are included in the LCA and TEA for all studied hydrogen production methods.

The flash H<sub>2</sub> process provides improvements in both cumulative energy demand (33–95% less energy) and greenhouse gas emissions (65–89% less emissions) when compared to other waste plastic or biomass deconstruction methods for H<sub>2</sub> production (Figure 5g,h). Despite the FeAlO<sub>x</sub>/microwave deconstruction producing less than stoichiometric CO<sub>2</sub> for polyolefins, the process still produces significant emissions producing the required weight equivalent of a metal complex. Flash H<sub>2</sub> production compares favorably to current industrial methods, producing 84% less greenhouse gas emissions than steam methane reforming, while using 4% less energy than green H<sub>2</sub>.

## 3. Conclusion

Since valuable turbostratic graphene is produced as a by-product of the FJH method, this provides a secondary value stream to improve the economic competitiveness of flash H<sub>2</sub> production. For the purposes of this TEA, the sale of this graphene is assumed at \$3 per kg, similar to the current cost of natural rubber and only 5% of the current market value of graphene (US\$60 per kg) to present a “worst-case” scenario. Preliminary estimated cost for the flash H<sub>2</sub> with graphene sale demonstrates that production costs are negative, −\$4.24 per kg H<sub>2</sub>, even at this unrealistically low sale price of graphene (Figure 5i). The FeAlO<sub>x</sub> catalyzed microwave deconstruction, despite producing high-value multiwalled carbon nanotubes with a higher simulated sale price of \$16 per kg, still exhibits high production costs due to the energy-intensive microwave use and large amount of metal required. Flash H<sub>2</sub> presents a new leading technology for H<sub>2</sub> production (Figure 5j). Our findings demonstrate that FJH can be leveraged to produce negative-cost clean H<sub>2</sub> from waste materials. Increased understanding of the FJH mechanism and improvements in scalability should help further optimize the flash H<sub>2</sub> production.

## 4. Experimental Section

**Materials:** Amorphous CB Pearls BP-2000 (Cabot), metallurgical coke (SunCoke), charcoal (EnviroSupply & Service), and waste plastic pyrolysis ash treated at 540 °C (Shangqiu Zhongming Eco-Friendly Equipment Co., Ltd in Shangqiu City, Henan, China) were used as received. Plastic waste was collected from household waste, including carbonated beverage bottles (PET), milk jugs (HDPE), grocery bags (LDPE), food packaging (PS), coffee cups (PP), piping (PVC), CD cases (PC), and LEGO bricks (ABS). Plastic waste was ground using an electric hammer mill (CGoldenWall, Model DF-15) and was sieved to only use particles smaller than 1 mm (#18 sieve). Pluronic-F127, a non-ionic surfactant, was obtained from Millipore-Sigma. Commercial graphene samples (H25 grade, XGScience) were used

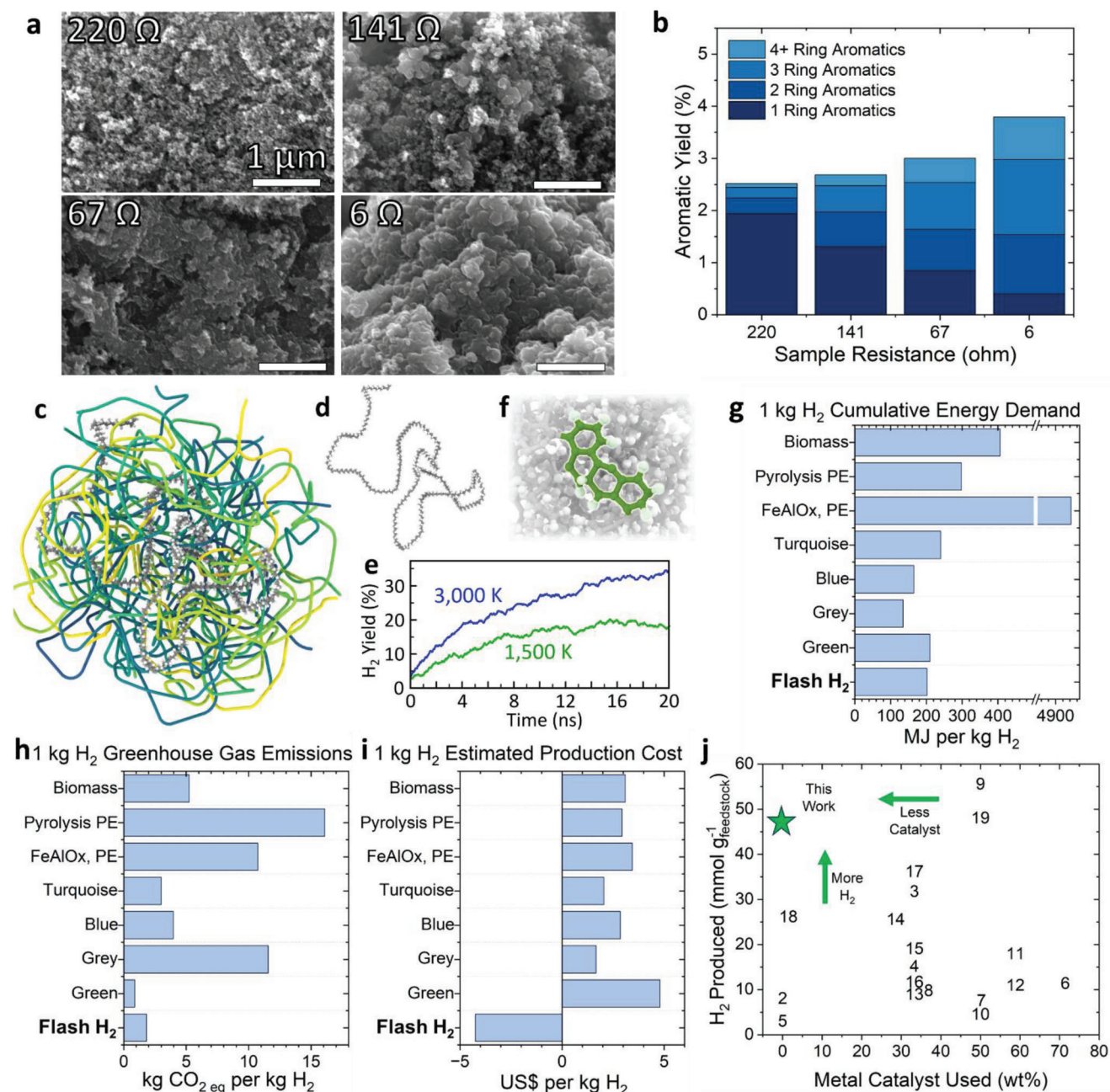


**Figure 5.** Mechanistic assessment of the catalyst-free FJH deconstruction process, and comparison to current industrial and laboratory methods. a) SEM micrographs examining the graphene morphology resulting from the deconstruction of HDPE as a function of initial resistance. All scale bars are the same. b) Aromatic products evolved, as a function of sample resistance, showing that aromatic formation and polymerization occur more readily at lower sample resistances. c–f) Atomistic simulations of the FJH reaction including c) a simplified representation of the atomistic model of a HDPE particle showing predominantly carbon spines of polymers where colors indicate individual polymer strands, d) an individual polymer strand in full atomistic details as extracted from c, e) H<sub>2</sub> production during the simulation at 1500 and 3000 K, and f) formation of aromatic networks at the early stages of HDPE deconstruction. g–i) The g) cumulative energy demand, h) greenhouse gas emissions, and i) estimated production cost resulting from the production of 1 kg H<sub>2</sub> using different methods. FJH PE is the flash Joule heating method to flash H<sub>2</sub> disclosed here. The data and source for each data point are available in Table S1a (Supporting Information). Key assumptions used here include that the power source for all is green energy, thus no emissions are contributed from powering each method. The FeAlO<sub>x</sub> PE process involves microwave irradiation. The estimated production cost of the FJH PE and FeAlO<sub>x</sub> PE processes includes the sale of high-value carbon coproducts. The estimated cost of the graphene is <5% of the current cost of bulk graphene. j) Comparing different methods that produce H<sub>2</sub> from waste plastic, biomass, or hydrocarbons. The numbers on the plot correspond to the row of the source data in Table S1b (Supporting Information). The data and source for each data point are available in Table S1b (Supporting Information).

without further purification. HPLC-grade hexane, toluene, and acetone, used for rinsing the waxes and oils from the volatile gas trap were used as received. Standard gas mixtures used for calibration and quantification of reaction products, and high-purity carrier gases, were obtained from Air-Gas. Standard hydrocarbon mixtures and polyaromatic hydrocarbon mixtures were used to characterize and quantify the oils and waxes produced.

**Methods:** The reaction precursors included 1) the postconsumer plastic ground by hammer mill (CGoldenWall, Model DF-15) and filtered through a 1.5 mm sieve and used without the need for any rinsing or pre-treatment, and 2) a small amount of conductive additive which might include graphite, graphene, metcoke, carbon black, etc. As demonstrated in Figure 2b the amount of conductive additive (in that plot it was Carbon Black BP-2000, Cabot), determined the initial resistance of the sample which impacted the temperature of the FJH reaction. When other conductive additives, such as pyrolysis, metcoke, or charcoal were used, a larger wt.% of conductive additive might be required to reach an equivalent resistance. Similarly, if smaller grain-size feedstocks such as asphaltene powders were used, then a larger amount of conductive additive had to be used. The amount of additive required was determined by the particle size and conductivity of the additive as well as the feedstock. Once the reaction precursors were mixed thoroughly by mortar and pestle, the resulting black/gray powder mixture could undergo the flash Joule heating process. Flash Joule heating the mixture of precursors is shown in Figure 2a, the mixture (0.5 g total, 0.08 g conductive additive Carbon Black BP-2000 from Cabot and 0.42 g polymer) was loaded into a quartz tube and compressed to have a resistance of 5–10 Ohm. A pellet of copper wool was used as an electrode to allow for gas escape, and a graphite rod acted as the electrode on the other side. The metal electrodes had sealing o-rings to create a gas-tight seal. A hollow electrode was required to allow for the release and capture of volatiles in a Pyrex Schlenk flask that was flushed with Ar and evacuated to  $-75$  kPa of vacuum. The entire system was leak-tight, holding the vacuum for at least  $\approx 15$  min after the valve to the vacuum was closed. Images of the system are shown below as reproduced from previous work.<sup>[17]</sup>

Then, flash Joule heating occurs, by charging a capacitor bank (220 mF) to 100–130 V. This was then discharged through the sample at very fast rates (typically less than 3 s) either using complete and non-modulated discharge. This process was repeated 3–4 times, until a singular sharp current discharge pulse was observed (inset in Figure 2a) and no more gas was evolved, as judged by a pressure gauge attached to the volatile trap. The interruptions in current discharge in the first 3 pulses were a result of volatiles leaving the system, temporarily increasing the resistance of the sample, thus lowering the amount of current able to pass through the sample. A pressure gauge attached to the volatile trap was used to measure the amount of volatiles that evolved. A gas chromatography-thermal conductivity detector (GC-TCD) was then used to measure the partial pressure of  $H_2$  in the mixture, which could then be used to determine the amount of  $H_2$  evolved by the process using the ideal gas equation and the experimentally determined pressure, temperature, and volume of evolved gases. GC-TCD could also detect methane and CO, if present. Syringe headspace sampling of the volatile trap was also analyzed by GC-MS, which detected and quantified the small hydrocarbons produced (up to  $C_6$  species) as well as  $CO_2$  and water. The volatile trap could also be rinsed with a variety of solvents to study oil, wax, or aromatic species by injecting this rinse into the GC-MS. Standard analyte mixtures (of gases, oils, and aromatics) allowed for the quantification of substances produced by the FJH deconstruction of plastics. The resulting graphene powder could be removed from the quartz tube, weighed, and characterized after grinding briefly by mortar and pestle and used without purification. The resulting hydrocarbon gas, oil, and wax minor byproducts expectedly varied with polymer identity, and some monomers, dimers, or oligomers of the parent polymers could be observed.

**Characterization Methods:** Gaseous products were analyzed using an Agilent 8890 GC with 5977 B MSD and G4407 TCD. A carrier gas of Ar was used for the TCD to allow accurate  $H_2$  detection, while a carrier gas of He was used for MSD analysis. The instrument was equipped with an Agilent HP-5 ms low-bleed column (30 m, 0.25 mm internal diameter, 0.25  $\mu$ m film). For permanent gas analysis, the instrument equipped with two Ag-

ilent 0.5 m HayeSep Q packed columns in series (Agilent part number G3591-82023), followed by an Agilent 2.44 m 5 Å MolSieve column (Agilent part number G3591-81022), using a carrier gas of Ar. Quantification of compounds was conducted using high-purity standard gas or analyte mixtures, using peak integration to determine unknown concentrations.

Raman spectra were collected using a Renishaw inVia Raman microscope outfitted with a 5 mW 532 nm laser. A 50 $\times$  objective lens was used to collect all spectra. Analysis of Raman spectra, including peak intensity ratios, utilized the height of the peak. Custom Python scripts were used to analyze Raman spectral mapping data. Briefly, spectra were smoothed using a Savitsky–Golay filter, background-corrected using a polynomial fit, and averaged to give bulk sample characteristics. The LiveTrack software was automatically used to adjust focus between spectra. If a G peak could not be identified within the collected spectrum, the spectrum was assumed to be poorly focused and was not employed in the analysis. This occurred  $<3\%$  of the time. XPS data was collected using a PHI Quantera SXM Scanning X-Ray Microprobe with a base pressure of  $5 \times 10^{-9}$  Torr. Survey spectra were recorded using 0.5 eV step sizes with a pass energy of 140 eV. Elemental spectra were recorded using 0.1 eV step sizes with a pass energy of 26 eV. All the XPS spectra were corrected using the C 1s peaks (284.6 eV) as reference. TGA thermograms were collected using a TA Instruments Q-600 Simultaneous TGA/DSC using alumina pans, with a heating rate of 5  $^{\circ}C$   $min^{-1}$  up to 780  $^{\circ}C$ . Air atmosphere at a flow rate of 80  $mL$   $min^{-1}$  was used to purge the sample chamber. Powder XRD spectra were collected using a Rigaku SmartLab II using zero background sample holders at a scan rate of 1 $^{\circ}$   $min^{-1}$  and a 0.05 $^{\circ}$  step size. SEM images were taken with a FEI Helios Nanolab 660 Dual Beam SEM System. A voltage of 15 keV was employed in imaging. TEM and SAED images were obtained on a JEOL 2100 field emission transmission electron microscope at an acceleration voltage of 200 kV. Samples were prepared by drop-casting extremely dilute graphene/ethanol solutions onto lacey carbon grids.

**Dispersibility Testing:** Graphene was dispersed in a 1% surfactant aqueous solution using Pluronic-F127, a non-ionic polyol surfactant. Varying amounts of ground graphene powder were weighed into centrifuge tubes, and the solvent was added to yield the initial loading concentration ( $\approx 1$  mg graphene powder  $mL^{-1}$  of solvent). The centrifuge tubes were then sonicated in a cup-horn sonicator for 10 min (Cole-Parmer Qsonica 448) and centrifuged at 550 relative centrifugal force for 5 min to remove larger aggregates. The supernatant was decanted after centrifugation and diluted 100 $\times$  since the graphene concentration led to a very high absorbance. The absorbance of the solution was measured at 660 nm. The concentration was determined using Beer's Law with an extinction coefficient of 66  $L$   $g^{-1}$   $cm^{-1}$ .

**Life-Cycle Assessment and Techno-Economic Assessment:** A cradle-to-gate ISO complaint life-cycle assessment consisted of a systematic analysis of the demands and impacts associated with a product from raw materials required for synthesis to the processing and manufacturing of the product and did not examine the final disposal of reaction by-products or consider the end-use application or disposal of the product. The specific goal of this life-cycle assessment was to evaluate the demands and environmental impacts resulting from the FJH production of  $H_2$  to compare with literature benchmarks studying the production of  $H_2$  synthesized using other methods. The system considered here covers three main steps: raw material production, reaction feedstock preparation, and FJH or microwave reaction. Transportation of raw materials was not considered here, and a lab-scale process was assumed. The functional unit considered here was 1 kg of high-purity  $H_2$ . The environmental impacts pertaining to the production of waste polyethylene were not considered in this study since it was a waste product and its demands or impacts were attributed to the primary use; however, the burdens for collection and separation of postconsumer waste polyethylene were included.<sup>[48]</sup> Direct energy inputs for the FJH process were measured experimentally (Figure S27, Supporting Information), and cumulative demands and impacts were calculated using Argonne National Laboratory GREET life-cycle assessment. Direct comparison of our life-cycle assessment with other literature values was possible if all databases utilized (e.g., GREET, SimaPro, Ecoinvent, and Gabi) followed the International Standards Organization's best standard

procedures. Literature values presented in this discussion all comply with this requirement.

Key assumptions used when conducting the FJH and FeAlO<sub>x</sub>/microwave LCAs herein include that the power source for these methods, like with green hydrogen electrolysis, was renewable energy, and that thus no emissions or water use were contributed from powering each method. The amount of greenhouse gases emitted was thus a result of sourcing and preparation of materials and any CO<sub>2</sub> produced stoichiometrically by the process. A sale price of US\$16 000 per ton was assumed for the MWCNT, as significant purification would be required to remove the reported ≈10–30 wt.% of catalyst. A “worst case” scenario was assumed for the sale price of graphene, at US\$3000 per ton, to account for possible market saturation. This assumed sale price of graphene at US\$3000 per ton was 95% lower than the actual current market value of multi-layered graphene products (US\$60 000 per ton). The cost of post-consumer HDPE was considered in the techno-economic analysis. An estimated overhead cost of capital expenses and operating expenses was based on averages of work done by Lan and Yao for 2000 tons of plastic processed per day basis factory (\$1.20 per kg H<sub>2</sub>),<sup>[12]</sup> as well as work done by the National Renewable Energy Labs for 500 tons of biomass processed per day basis factory (\$3.10 per kg H<sub>2</sub>).<sup>[49]</sup> Overhead costs could be accurately modeled using software such as Aspen Plus, but this was deemed beyond the scope of this current work. Further LCA details and scenarios are presented in Figure S11 and Table S2 (Supporting Information).

**Computational Methods:** The initial configuration of the atomistic model of HDPE particles was created by generating one carbon chain at a time, where each chain was composed of straight and curved segments of random length between 3 and 8 carbon atoms and curved segments displaying deviation from the straight line in randomized direction with angle up to 60° per carbon atom. The direction of the polymer chains was adjusted if the distance to any chain was found to be lower than 3.4 Å. Any chain shorter than 150 atoms was discarded to prevent structural unraveling during MD simulation. Hydrogen atoms were iteratively added after all carbon chains were generated. The final structure contained ≈16 000 atoms. To allow the generation of H<sub>2</sub> and other gases, the periodic box significantly exceeded the size of the HDPE particle and was set to 300 Å in all directions.

The MD simulations were carried out with AIREBO interatomic potential,<sup>[42,43]</sup> as implemented in the LAMMPS package.<sup>[50]</sup> To eliminate any possible artifacts introduced during structure creation, the initial configuration was subjected to geometric optimization followed by the annealing at 400 K for 5 × 10<sup>-9</sup> s. The structure was then heated to target temperatures (1500 and 3000 K) with the heating speed of 0.5 × 10<sup>-12</sup> K s<sup>-1</sup> using a Nose–Hoover thermostat (canonical NVT ensemble) with a temperature damping parameter of 0.025 × 10<sup>-12</sup> s and was held at the target annealing temperatures for 20 × 10<sup>-9</sup> s.

**Ethics Declaration:** Rice University owns the intellectual property (IP) on the process to generate flash H<sub>2</sub> from plastic waste, and that IP is currently unlicensed. Universal Matter Inc. has licensed IP from Rice University on the synthesis of graphene from carbon sources. JMT is a stockholder in that company, but not an officer, director, or employee. Conflicts of interest are mitigated through compliance and reporting with the Rice University Office of Sponsored Programs and Research Compliance.

## Supporting Information

Supporting Information is available from the Wiley Online Library or from the author.

## Acknowledgements

The authors acknowledge the Rice Electron Microscope Center (EMC) for consultation and instrument maintenance. JMT and BYI thank the US Army Corps of Engineers, ERDC, for their support (W912HZ-21-2-0050). J.M.T. also thanks the Air Force Office of Scientific Research (FA9550-22-1-0526). K.M.W. and J.L.B. thank the National Science Foundation for Grad-

uate Research Fellowship Program funding. K.V.B. and B.I.Y. additionally thank the Office of Naval Research (N00014-22-1-2788).

## Conflict of Interest

The authors declare no conflict of interest.

## Data Availability Statement

The data that support the findings of this study are available from the corresponding author upon reasonable request.

## Keywords

clean hydrogen production, flash hydrogen, waste plastics, zero cost clean hydrogen

Received: July 10, 2023  
Revised: August 24, 2023  
Published online: October 25, 2023

- [1] A. Ajanovic, M. Sayer, R. Haas, *Int. J. Hydrogen Energy* **2022**, *47*, 24136.
- [2] S. Van Renssen, *Nat. Clim. Change* **2020**, *10*, 799.
- [3] S. A. Grigoriev, V. N. Fateev, D. G. Bessarabov, P. Millet, *Int. J. Hydrogen Energy* **2020**, *45*, 26036.
- [4] S. Shiva Kumar, H. Lim, *Energy Rep.* **2022**, *8*, 13793.
- [5] Z. J. Baum, L. L. Diaz, T. Konovalova, Q. A. Zhou, *ACS Omega* **2022**, *7*, 32908.
- [6] R. R. Beswick, A. M. Oliveira, Y. Yan, *ACS Energy Lett.* **2021**, *6*, 3167.
- [7] M. Hermesmann, T. E. Müller, *Prog. Energy Combust. Sci.* **2022**, *3*, 300, 100996.
- [8] R. W. Howarth, M. Z. Jacobson, *Energy Sci. Eng.* **2021**, *9*, 1676.
- [9] N. Sazali, *Int. J. Hydrogen Energy* **2020**, *45*, 18753.
- [10] “Hydrogen Shot,” can be found under <https://www.energy.gov/eere/fuelcells/hydrogen-shot> (accessed: August 2023).
- [11] J. M. Garcia, M. L. Robertson, *Science* **2017**, *358*, 870.
- [12] K. Lan, Y. Yao, *Commun. Earth Environ.* **2022**, *3*, 300.
- [13] N. Cai, X. Li, S. Xia, L. Sun, J. Hu, P. Bartocci, F. Fantozzi, P. T. Williams, H. Yang, H. Chen, *Energy Convers. Manage.* **2021**, *229*, 113794.
- [14] X. Jie, W. Li, D. Slocombe, Y. Gao, I. Banerjee, S. Gonzalez-Cortes, B. Yao, H. Almegren, S. Alshihri, J. Dilworth, J. Thomas, T. Xiao, P. Edwards, *Nat. Catal.* **2020**, *3*, 902.
- [15] D. X. Luong, K. V. Bets, W. A. Algozeeb, M. G. Stanford, C. Kittrell, W. Chen, R. V. Salvatierra, M. Ren, E. A. Mchugh, P. A. Advincula, Z. Wang, M. Bhatt, H. Guo, V. Mancevski, R. Shahsavari, B. I. Yakobson, J. M. Tour, *Nature* **2020**, *577*, 647.
- [16] W. Chen, J. T. Li, Z. Wang, W. A. Algozeeb, D. X. Luong, C. Kittrell, E. A. Mchugh, P. A. Advincula, K. M. Wyss, J. L. Beckham, M. G. Stanford, B. o Jiang, J. M. Tour, *ACS Nano* **2021**, *15*, 11158.
- [17] W. A. Algozeeb, P. E. Savas, D. X. Luong, W. Chen, C. Kittrell, M. Bhat, R. Shahsavari, J. M. Tour, *ACS Nano* **2020**, *14*, 15595.
- [18] K. M. Wyss, R. D. De Kleine, R. L. Couvreur, A. Kiziltas, D. F. Mielewski, J. M. Tour, *Commun. Eng.* **2022**, *1*, 3.
- [19] K. M. Wyss, W. Chen, J. L. Beckham, P. E. Savas, J. M. Tour, *ACS Nano* **2022**, *16*, 7804.
- [20] K. M. Wyss, B. Deng, J. M. Tour, *Nano Today* **2023**, *49*, 101781.
- [21] S. K. Tiwari, S. Sahoo, N. Wang, A. Huczko, *J. Sci.: Adv. Mater. Devices* **2020**, *5*, 10.

- [22] M. J. Allen, V. C. Tung, R. B. Kaner, *Chem. Rev.* **2010**, *110*, 132.
- [23] K. M. Wyss, D. X. Luong, J. M. Tour, *Adv. Mater.* **2022**, *34*, 2106970.
- [24] O. Li, S. Tamrakar, Z. Iyigundogdu, D. Mielewski, K. Wyss, J. M. Tour, A. Kiziltas, *Polym. Compos.* **2022**, *44*, 1494.
- [25] P. A. Advincula, V. Granja, K. M. Wyss, W. A. Algozeeb, W. Chen, J. L. Beckham, D. X. Luong, C. F. Higgs, J. M. Tour, *Carbon* **2023**, *203*, 876.
- [26] A. P. Kauling, A. T. Seefeldt, D. P. Pisoni, R. C. Pradeep, R. Bentini, R. V. B. Oliveira, K. S. Novoselov, A. H. Castro Neto, *Adv. Mater.* **2018**, *30*, 1803784.
- [27] C. Backes, A. M. Abdelkader, C. Alonso, A. Andrieux-Ledier, R. Arenal, J. Azpeitia, N. Balakrishnan, L. Banszerus, J. Barjon, R. Bartali, S. Bellani, C. Berger, R. Berger, M. M. B. Ortega, C. Bernard, P. H. Beton, A. Beyer, A. Bianco, P. Boggild, F. Bonaccorso, G. B. Barin, C. Botas, R. A. Bueno, D. Carriazo, A. Castellanos-Gomez, M. Christian, A. Ciesielski, T. Ciuk, M. T. Cole, J. Coleman, et al., *2D Mater.* **2020**, *7*, 022001.
- [28] A. C. Ferrari, D. M. Basko, *Nat. Nanotechnol.* **2013**, *8*, 235.
- [29] K. M. Wyss, J. T. Li, P. A. Advincula, K. V. Bets, W. Chen, L. Eddy, K. J. Silva, J. L. Beckham, J. Chen, W. Meng, B. Deng, S. Nagarajaiah, B. I. Yakobson, J. M. Tour, *Adv. Mater.* **2023**, *35*, 2209621.
- [30] S. Shallcross, S. Sharma, E. Kandelaki, O. A. Pankratov, *Phys. Rev. B* **2010**, *81*, 165105.
- [31] Y. Cao, V. Fatemi, S. Fang, K. Watanabe, T. Taniguchi, E. Kaxiras, P. Jarillo-Herrero, *Nature* **2018**, *556*, 43.
- [32] K. M. Wyss, Z. Wang, L. B. Alemany, C. Kittrell, J. M. Tour, *ACS Nano* **2021**, *15*, 10542.
- [33] K. M. Wyss, J. L. Beckham, W. Chen, D. X. Luong, P. Hundi, S. Raghuraman, R. Shahsavari, J. M. Tour, *Carbon* **2021**, *174*, 430.
- [34] "Universal Matter Material Science: Graphene In A Flash," can be found under <https://www.universalmatter.com/> (accessed: August 2023).
- [35] J. C. Petersen, in *Development in Petroleum Science*, (Eds.: T. F. Yen, G. V. Chilingarian), Elsevier, Amsterdam, Netherlands **2000**, ch. 2.
- [36] M. G. Stanford, K. V. Bets, D. X. Luong, P. A. Advincula, W. Chen, J. T. Li, Z. Wang, E. A. Mchugh, W. A. Algozeeb, B. I. Yakobson, J. M. Tour, *ACS Nano* **2020**, *14*, 13691.
- [37] J. L. Beckham, K. M. Wyss, Y. Xie, E. A. Mchugh, J. T. Li, P. A. Advincula, W. Chen, J. Lin, J. M. Tour, *Adv. Mater.* **2022**, *34*, 2106506.
- [38] F. Kokai, M. Ishihara, A. Koshio, A. Nakayama, Y. Koga, *Diamond Relat. Mater.* **2007**, *16*, 1264.
- [39] L. C. Lopes, L. C. Da Silva, B. G. Vaz, A. R. M. Oliveira, M. M. Oliveira, M. L. M. Rocco, E. S. Orth, A. J. G. Zabin, *Chem. Sci.* **2018**, *9*, 7297.
- [40] I. J. Webster, J. L. Beckham, N. D. Johnson, M. A. Duncan, *J. Phys. Chem. A* **2022**, *126*, 1144.
- [41] C. S. Contreras, F. Salama, *Astrophys. J. Suppl. Ser.* **2013**, *208*, 6.
- [42] S. J. Stuart, A. B. Tutein, J. A. Harrison, *J. Chem. Phys.* **2000**, *112*, 6472.
- [43] D. W. Brenner, O. A. Shenderova, J. A. Harrison, S. J. Stuart, B. Ni, S. B. Sinnott, *J. Phys. Condens. Matter* **2002**, *14*, 783.
- [44] M. S. Miao, M.-L. Zhang, V. E. Van Doren, C. Van Alsenoy, J. L. Martins, *J. Chem. Phys.* **2001**, *115*, 11317.
- [45] K. V. Bets, B. I. Yakobson, *Nano Res.* **2009**, *2*, 161.
- [46] S. Hellweg, L. Milà I Canals, *Science* **2014**, *344*, 1109.
- [47] Y. Khojasteh Salkuyeh, B. A. Saville, H. L. Maclean, *Int. J. Hydrogen Energy* **2017**, *42*, 18894.
- [48] M. A. Martín-Lara, J. A. Moreno, G. Garcia-Garcia, S. Arjandas, M. Calero, *J. Clean Prod.* **2022**, *365*, 132625.
- [49] M. Ruth, Hydrogen Production Cost Estimate Using Biomass Gasification: Independent Review, United States: N P, **2011**, <https://doi.org/10.2172/1028523> (accessed: July 2023).
- [50] A. P. Thompson, H. M. Aktulga, R. Berger, D. S. Bolintineanu, W. M. Brown, P. S. Crozier, P. J. In 'T Veld, A. Kohlmeyer, S. G. Moore, T. D. Nguyen, R. Shan, M. J. Stevens, J. Tranchida, C. Trott, S. J. Plimpton, *Comput. Phys. Commun.* **2022**, *271*, 108171.